Thin-Film Morphology of Inkjet-Printed Single-Droplet Organic Transistors Using Polarized Raman Spectroscopy: Effect of Blending TIPS-Pentacene with Insulating Polymer

David T. James,[†] B. K. Charlotte Kjellander,[‡] Wiljan T. T. Smaal,[‡] Gerwin H. Gelinck,[‡] Craig Combe,[§] Iain McCulloch,[§] Richard Wilson,[⊥] Jeremy H. Burroughes,[⊥] Donal D. C. Bradley,[†] and Ji-Seon Kim[†,¶,*]

[†]Department of Physics and Centre for Plastic Electronics, Imperial College London, London SW7 2AZ, United Kingdom, [‡]Holst Centre/TNO, High Tech Campus 31, 5656 AE Eindhoven, The Netherlands, [§]Department of Chemistry and Centre for Plastic Electronics, Imperial College London, London SW7 2AZ, United Kingdom, [⊥]Cambridge Display Technology Ltd., Cambourne Business Park, Cambridgeshire CB23 6DW, United Kingdom, and [¶]Department of Materials Science and Engineering, KAIST, Daejeon 305-701, Republic of Korea

ABSTRACT

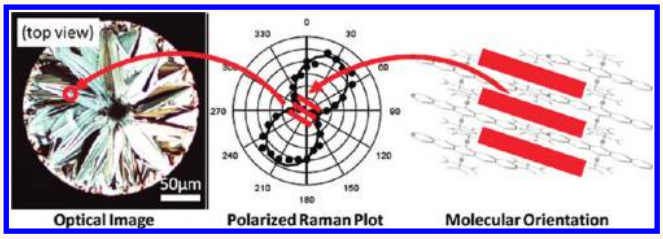

We report thin-film morphology studies of inkjet-printed single-droplet organic thin-film transistors (OTFTs) using angle-dependent polarized Raman spectroscopy. We show this to be an effective technique to determine the degree of molecular order as well as to spatially resolve the orientation of the conjugated backbones of the 6,13-bis(triisopropylsilylethynyl)-pentacene (TIPS-Pentacene) molecules. The addition of an insulating polymer, polystyrene (PS), does not disrupt the $\pi-\pi$ stacking of the TIPS-Pentacene molecules. Blending in fact improves the uniformity of the molecular morphology and the active layer coverage within the device and reduces the variation in molecular orientation between polycrystalline domains. For OTFT performance, blending enhances the saturation mobility from 0.22 ± 0.05 cm^2/(V·s) (TIPS-Pentacene) to 0.72 ± 0.17 cm^2/(V·s) (TIPS-Pentacene:PS) in addition to improving the quality of the interface between TIPS-Pentacene and the gate dielectric in the channel, resulting in threshold voltages of $\sim$0 V and steep subthreshold slopes.

KEYWORDS: organic transistors · pentacene · inkjet printing · morphology · Raman spectroscopy

Recent work on small-molecule-based organic thin-film transistors (OTFTs) has focused on controlling the morphology of the organic semiconductor material in the thin active layer next to the gate dielectric, thus improving charge carrier mobilities and reducing the variability between devices fabricated using the same process. One such technique is to use organic small-molecule–insulating polymer blends[1−3] as the active layer in solution-processed OTFTs in an effort to harness both the intrinsic high mobilities of small molecules[4] and the stabilizing effect of polymers. Despite advances in OTFT research, there remain numerous scientific challenges in device optimization and characterization including, among others, understanding the molecular orientation within the active channel and the role of domain boundaries and uniformity within and between devices.[5] Establishing a deeper understanding of the thin-film morphology of organic layers in device structures and relating this to charge transport properties would provide a more solid grounding with which to improve OTFT fabrication techniques and, thus, performance.

TIPS-Pentacene has proven to be a useful material to explore OTFT fabrication techniques including spin-coating,[1] drop-casting,[6] dip-coating,[7] and inkjet printing.[8] Inkjet printing particularly is a well-established technique in the controlled deposition of organic semiconductor inks for the fabrication of OLED displays due to advantages such as efficiency of material use, high-resolution patterning, good reproducibility, and ease of scalability.[9] The use of inkjet printing for small-molecule/polymer blend OTFTs is relatively new[10] and would benefit from a better understanding of the morphology that evolves for the active ink droplet in the device. For example, small-molecule/polymer blends[2,3] have been shown to improve

* Address correspondence to ji-seon.kim@imperial.ac.uk.

Received for review September 2, 2011 and accepted October 27, 2011.

Published online October 28, 2011
10.1021/nn203397m

device-to-device uniformity and ease of processing while retaining high mobilities in the active layer. They also allow fabrication of high-performance organic integrated circuits.[11] While improvements in morphology have been monitored by optical and scanning probe microscopies and inferred by better device characteristics, one of the problems is to understand in full the structural basis of these improvements.[12] Work has been done on the vertical structure of blend devices showing segregation of small-molecular material at the top and bottom interfaces;[3,8,13−15] however, there is a need for further study on the lateral morphology of small-molecular OTFTs and how this relates to device performance. As a consequence, additional probes of the spatially resolved morphology of the active layer in OTFT device structures would be highly desirable. In this regard, we note that micro-Raman spectroscopy has proven to be a useful tool in determining the morphology of organic semiconductor thin films.[16−20] In addition to a high spatial resolution (~1 μm compared to ~10 μm in FT-IR), Raman spectroscopy is a simple, nondestructive technique that requires no previous sample preparation and allows for the *in situ* characterization of even working devices.[21,22] Angle-dependent polarized Raman spectroscopy can be used to look at the local molecular alignment of polycrystalline thin films deposited using alignment techniques such as zone-casting.[23] The primary advantage of Raman spectroscopy over other structural analysis techniques such as XRD is the ability to map out local changes in molecular structure rather than measuring the "average" picture of a thin film or device.

In this paper, we report on the application of polarized Raman spectroscopy to the characterization of local molecular order and orientation of TIPS-Pentacene thin films deposited using the inkjet printing method. We study first the effect of surface treatment of SiO_2 and gold substrates using self-assembled monolayers (SAMs), namely, trichlorophenylsilane (TCPS) and pentafluorobenzenethiol (PFBT). Second, we study the impact of blending an insulating polymer with the TIPS-Pentacene. Finally, we examine the dependence of varying the channel length on the local morphology (molecular order and orientation) of TIPS-Pentacene/blend thin films in device structures. These observations will then be correlated to transistor performance to elucidate the essential role that morphology plays.

RESULTS AND DISCUSSION

Raman Spectroscopy of TIPS-Pentacene. The Raman spectrum of a TIPS-Pentacene (single-droplet) thin-film, inkjet-printed on PFBT-treated gold, is shown in Figure 1a. The chemical structure of TIPS-Pentacene is shown in Figure 1b. By comparing the experimentally obtained spectrum with the calculated vibrational frequency spectrum (Supporting Information, Figure S1), Raman mode assignments were made as shown in Figure 1c. The calculated atomic displacement vectors are shown in the Supporting Information, Figure S2. The C−H bending modes (from the ends and sides of the pentacene backbone) assigned here are in good agreement with the equivalent previously assigned modes in pentacene thin films.[24−26] Additionally, two C−C ring stretch modes were assigned (1374 and 1578 cm^{-1}) with the carbon atoms predominantly vibrating along the short and long molecular axis, respectively (axes indicated in Figure 1b). Since the pentacene backbones are lying in the plane of the substrate,[27] these long- and short-axis modes (1374 and 1578 cm^{-1}) can be used to probe the in-plane orientations of the long- and short-axes of the pentacene backbones in the films. When the laser polarization aligns parallel to the short axis, a maximum Raman scattering intensity will be observed for the 1374 cm^{-1} (short-axis) mode, likewise, for the 1578 cm^{-1} (long-axis) mode. Experimentally, other modes also show high polarization anisotropy in ordered films (*e.g.*, C−H bending modes); however, the 1374 and 1578 cm^{-1} modes have the highest scattering intensities and therefore will be the focus of this paper.

To verify the orthogonality of these modes in polycrystalline TIPS-Pentacene thin films, the Raman intensities of both modes were measured as a function of polarization angle within a large crystalline TIPS-Pentacene domain (Figure 1d). Both peak intensities varied as $\cos^2(\theta)$, with the short- and long-axis modes being 90° out of phase as expected.

In order to demonstrate how powerful angle-dependent polarized Raman spectroscopy is, we use it here to distinguish between ordered/disordered regions in a thin film and furthermore to determine the degree of local molecular order in these regions. The Raman anisotropies of ordered/disordered regions for a thin film fabricated with a different pentacene derivative were first studied. Asymmetric 6-(triisopropylsilylethynyl)-13-(triethylsilylethynyl)pentacene (TIPS-TES-Pentacene) (chemical structure shown in Figure 2) was drop-cast from toluene solution on quartz at room temperature.

The resulting film was composed primarily of disordered material, with crystalline domains (size >100 μm) forming at the film edges. Representative Raman spectra (under 785 nm excitation) from the disordered and ordered regions are shown in Figure 2a. The features from the Raman spectrum are in good agreement with the TIPS-Pentacene Raman spectrum (Figure 1a), which is expected since the Raman modes in the region shown arise from vibrations within the pentacene backbone itself, rather than the bulky side groups. While the TIPS-TES-Pentacene Raman spectrum from the disordered region is accompanied by a fluorescence background, the spectrum from the

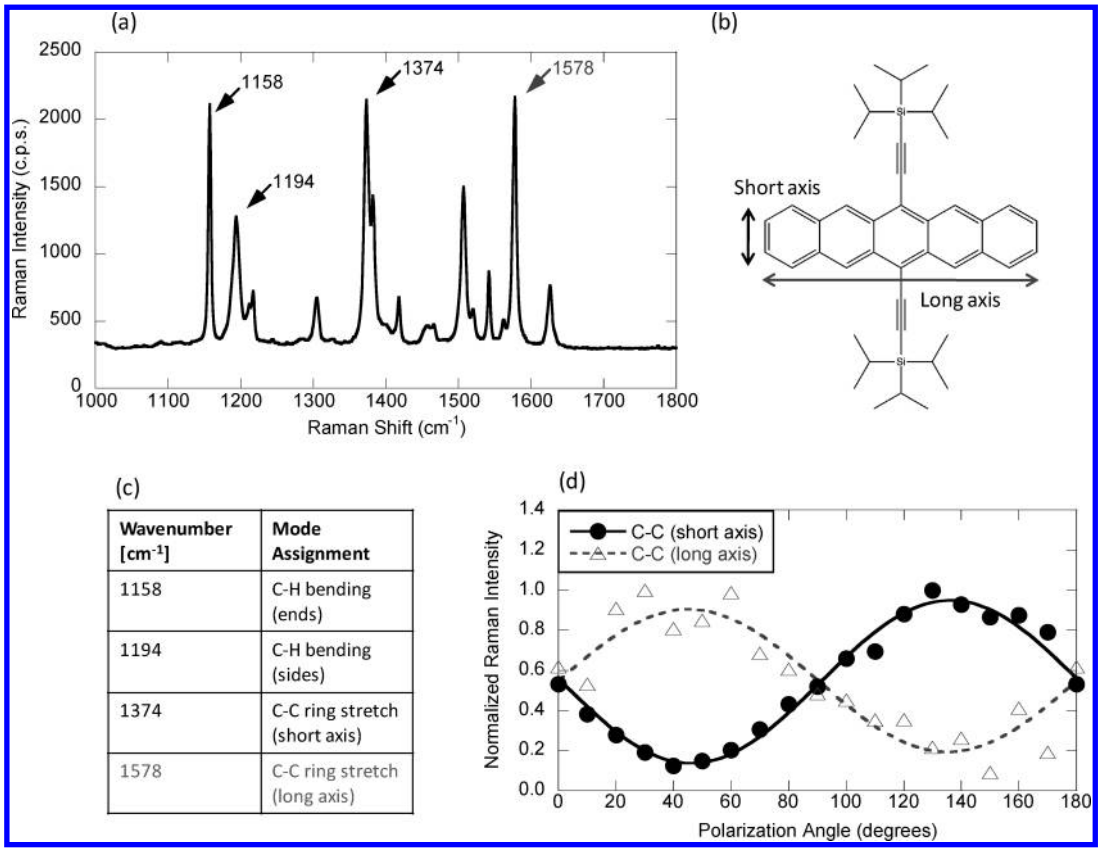

Wavenumber [cm^{-1}]	Mode Assignment
1158	C-H bending (ends)
1194	C-H bending (sides)
1374	C-C ring stretch (short axis)
1578	C-C ring stretch (long axis)

Figure 1. (a) Raman spectrum (under 785 nm excitation) of a TIPS-Pentacene thin-film inkjet-printed on a PFBT-treated gold substrate. At this excitation, no peaks from polystyrene are observed in TIPS-Pentacene:PS blend spectra; therefore, pristine and blend spectra are virtually identical. (b) TIPS-Pentacene chemical structure. (c) Raman mode assignments for the four predominant peaks, and (d) intensity of short- and long-axis Raman modes as a function of polarization angle.

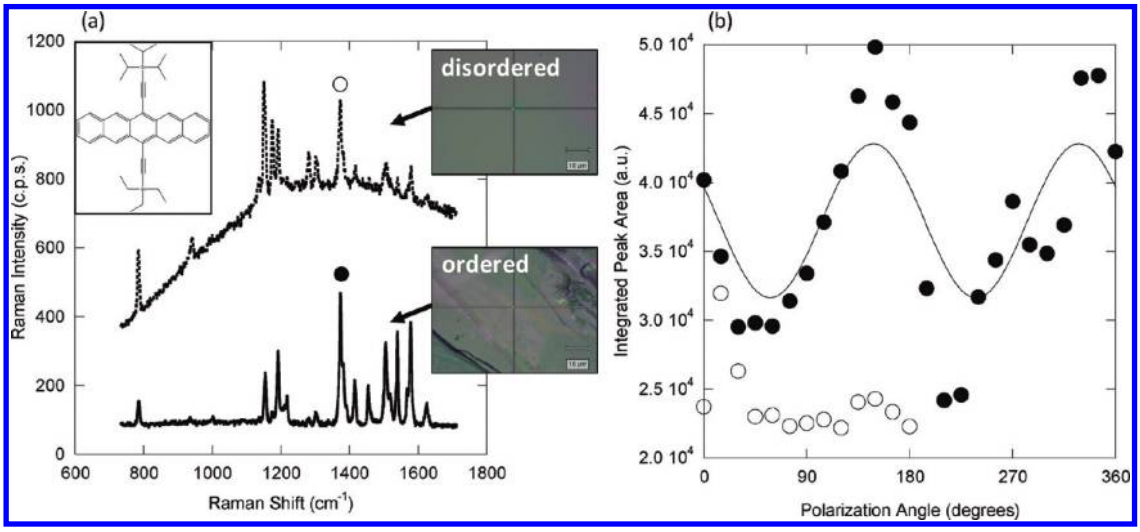

Figure 2. (a) Raman spectra of ordered (solid line) and disordered (dashed line) regions of a TIPS-TES-Pentacene film (optical images shown on graph). The TIPS-TES-Pentacene chemical structure is shown inset. (b) Integrated intensity of the C−C (short-axis) Raman mode in the ordered (●) and disordered (○) regions of the film as a function of incident polarization angle. A $\cos^2(\theta)$ curve fit (solid line) is shown for reference.

ordered region has dramatically reduced fluorescence background. The quenching of background fluorescence is characteristic of the formation of H-aggregates, which causes the splitting of the exciton bands such that the lower band becomes non-emissive, and has been previously reported for similar materials.[28,29] The intensity of the C−C (short-axis) mode is plotted as a function of polarization angle for both morphologies in Figure 2b.

The disordered phase showed no or very little anisotropy in the C−C (short-axis) mode intensity, while the ordered phase gave an anisotropy value of ~0.4. Quantifying the anisotropy (calculated using $(I_{MAX} - I_{MIN})/I_{MAX}$) gives an indication of the degree of molecular order (where $(I_{MAX} - I_{MIN})/I_{MAX} = 1$ for purely ordered phases and 0 for purely disordered phases), while the angular position of the maximum intensity (θ_{MAX}) gives an indication of the mean in-plane orientation of the pentacene backbones. By measuring the fluorescence background and vibrational transitions of the molecules, it is therefore possible to gain information about the molecular order and the morphology of the thin film, which are the main factors that determine the optical and charge transport properties of organic semiconductors and, therefore, the device performance of OTFTs.

Thin-Film Morphology Characterization. Initial morphology characterization was performed on single-droplet inkjet-printed TIPS-Pentacene thin films on unpatterned SAM-treated substrates. It is clear from the cross-polarized optical images (Figure 3 (left)) that the films deposited on a PFBT-treated gold substrate show a more pronounced appearance of large (>10 μm) crystalline domains growing radially inward from the droplet edge, compared to the more granular/disordered morphology of the films deposited on a TCPS-treated SiO_2 substrate.

Previous studies suggest that the different morphology from both substrates can be explained by the effect of surface energy on the drying dynamics of the droplets.[30,31] To gain further information on the degree of order in the different films, angle-dependent polarization plots of the C−C ring stretch (short-axis) mode, taken from within a single domain near the center of the droplet, are shown (Figure 3 (bottom)).

The films deposited on PFBT-treated gold substrate showed higher anisotropy (~0.84−0.87) than the films on TCPS-treated SiO_2 substrate (~0.27−0.33), consistent with the observations from the optical images. Higher anisotropy would indicate that, within the laser spot area, a larger proportion of the pentacene backbones are aligned in a common direction, that is, higher molecular order at the micrometer-scale. Studies have shown that TIPS-Pentacene molecules readily form crystalline domains in the solid state due to strong 2D $\pi-\pi$ stacking;[31] therefore, the change in molecular order here is attributed to a change in the size of TIPS-Pentacene crystallites. Randomly oriented crystallites much smaller than the laser spot-size would lead to very low Raman anisotropy, but crystallites with a size comparable to or larger than the laser spot would exhibit high Raman anisotropy. Comparing the TIPS-Pentacene and TIPS-Pentacene:PS droplets on PFBT-treated gold in plots (a) and (c), it was determined that the mean orientation of pentacene backbones within the domains probed was ~30 and ~60° from the vertical, respectively. Interestingly, within these domains, there is very little difference in the degree of molecular order between (neat) TIPS-Pentacene and TIPS-Pentacene:PS blend, suggesting that blending does not disrupt the $\pi-\pi$ stacking of TIPS-Pentacene molecules. Indeed, the blend film shows marginally higher anisotropy.

OTFT Morphology Characterization. Characterization of complete OTFTs was performed using a combination of optical and scanning probe microscopy and spatially resolved Raman spectroscopy. Figure 4 shows the cross-polarized optical images of 40 μm channel length OTFTs printed using (a) TIPS-Pentacene and (b) TIPS-Pentacene:PS inks. Optical microscopy provides a quick method to characterize the thin film. The droplet is surrounded by a thick rim of TIPS-Pentacene material, a so-called coffee stain effect.[32] The coffee stain rims and the center of the deposits appear brighter in the cross-polarized micrographs due to the larger amounts of birefringent crystals in these areas. The topography of a rectangular zone in the plane of the film (indicated by the red dashed line) was determined using atomic force microscopy (AFM) in noncontact mode (c,d). From the topography data, the rim thickness was determined to be 80−100 nm with the mean thickness of the polycrystalline region toward the center of the droplet being 20−30 nm thick.

To gain further understanding of the droplet film morphology, Raman line scans were performed (Figure 5) along the channel width and channel length directions (indicated by the red arrows) in both the TIPS-Pentacene (panel a) and TIPS-Pentacene:PS (panel b) OTFTs. From these line scans, the integrated intensities of both the pentacene backbone C−C short-axis (blue) and long-axis (red) modes were extracted and plotted as a function of distance across the droplet. Complementary height profiles (taken from the same regions as the Raman measurements) were then extracted from the AFM scans in order to compare with the Raman data.

TIPS-Pentacene. Along the channel width direction (vertical scan), the topography data (Figure 5a (left)) indicate that most of the OTFT is covered by a ~20 nm thick TIPS-Pentacene layer, with an ~80 nm thick rim and a void in the center. Turning to the Raman data (Figure 5a (right)), the spikes in the integrated Raman modes coming from the droplet edges are consistent with the thick rim seen in the topography data. Inside the droplet, however, there is a large variation in integrated C−C short-axis and long-axis mode intensities. Since the polarization vector of the incident laser light is aligned perpendicular to the gold contacts, pentacene backbones also oriented perpendicular to the contacts would give a high C−C (long-axis) mode intensity (and corresponding low C−C (short-axis) mode intensity), and backbones oriented parallel to the contacts would give a high C−C (short-axis) mode intensity (and corresponding low C−C (long-axis)

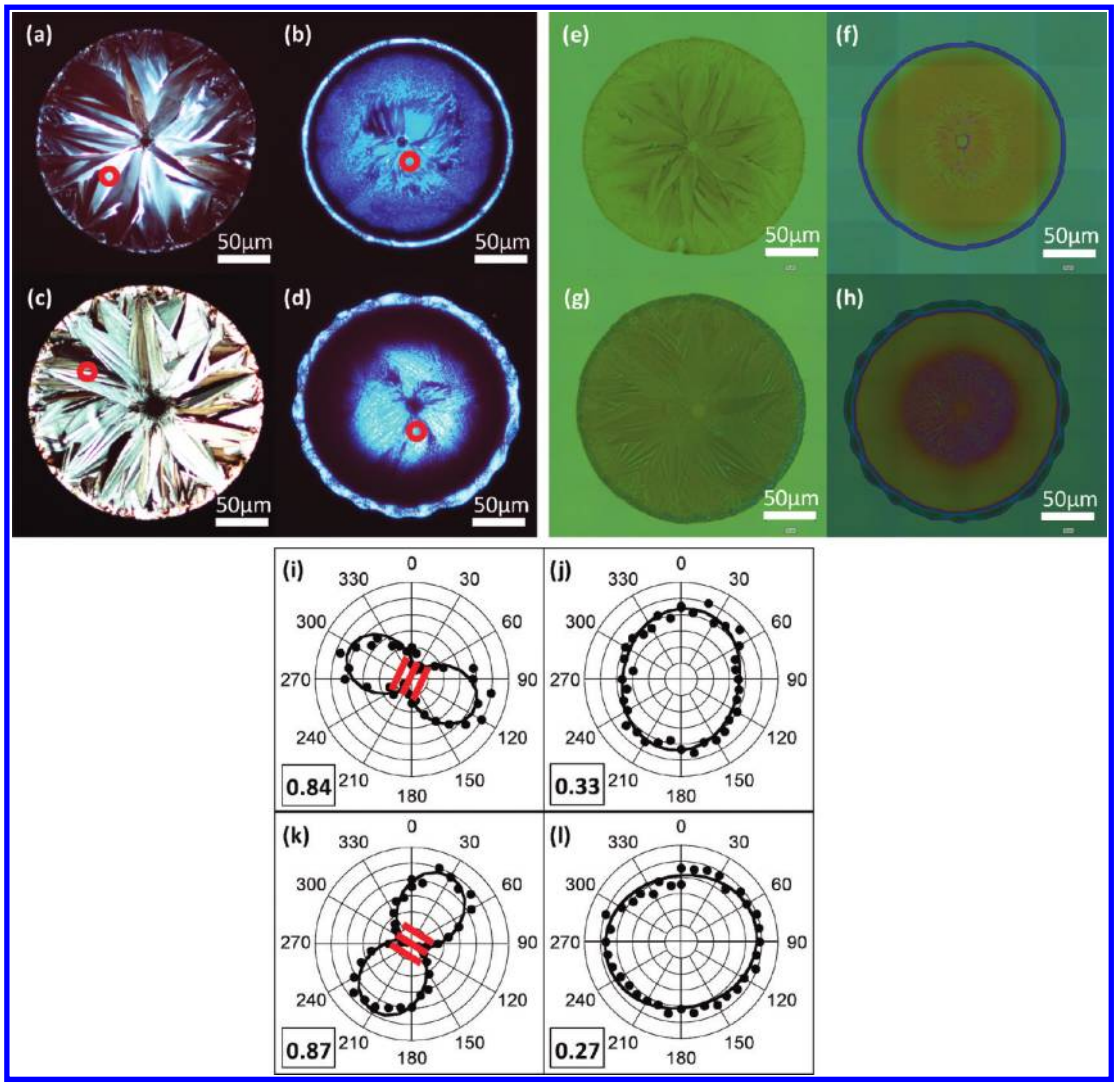

Figure 3. Optical (a–d) cross-polarized and (e–h) unpolarized images of inkjet-printed droplets containing (a,b) TIPS-Pentacene and (c,d) TIPS-Pentacene:PS blend deposited on (a,c) PFBT-treated gold and (b,d) TCPS-treated Si/SiO_2 substrates. (Bottom (i–l)) Raman intensity of the C–C ring stretch (short-axis) mode as a function of polarization angle, taken from points within a domain from each deposited droplet (circled red in (a–d)). Data from droplets deposited on gold/PFBT (i,k) show higher anisotropy than droplets deposited on Si/SiO_2/TCPS (j,l). Corresponding values of the anisotropy (($I_{MAX} - I_{MIN}$)/I_{MAX}) are recorded in the bottom left corner of each of the plots. Pentacene backbone orientations are indicated in red. The highest anisotropy is for TIPS-Pentacene:PS deposited on PFBT-treated gold (k) and the lowest for TIPS-Pentacene:PS on Si/SiO_2/TCPS (l).

mode intensity). By comparison with the cross-polarized optical image, it is evident that the C–C modes vary only gradually within a microcrystalline grain but change dramatically at the grain boundaries. This suggests that the pentacene backbones are ordered along a common direction within a grain and change abruptly in orientation between grains.

In order to more accurately determine the mean orientation of the pentacene backbones within the domains, a polarization rotation series was measured at the center of each crystalline domain (away from the grain boundaries). Measured pentacene backbone orientations are indicated in the figure, confirming the large variation in pentacene orientation between grains.

Along the channel length direction (horizontal scan), the topography is much more varied (Figure 5a (top)). The gold contacts can be seen as periodic ~30 nm high features (shaded in gold on the figure). The regions between the contacts (numbered in the figure) will now be described together with the Raman data (Figure 5a (bottom)). At contact 1, there is an accumulation of TIPS-Pentacene from the coffee stain rim and also an enhanced TIPS-Pentacene Raman signal. There are two main factors involved in the enhancement of the Raman signal: first, a higher Raman signal would be expected from a thicker region of the film (as observed in the topography), and second, there is an optical enhancement caused by the reflection of laser light from the gold. This would effectively increase the laser intensity in the exposed region and lead to an

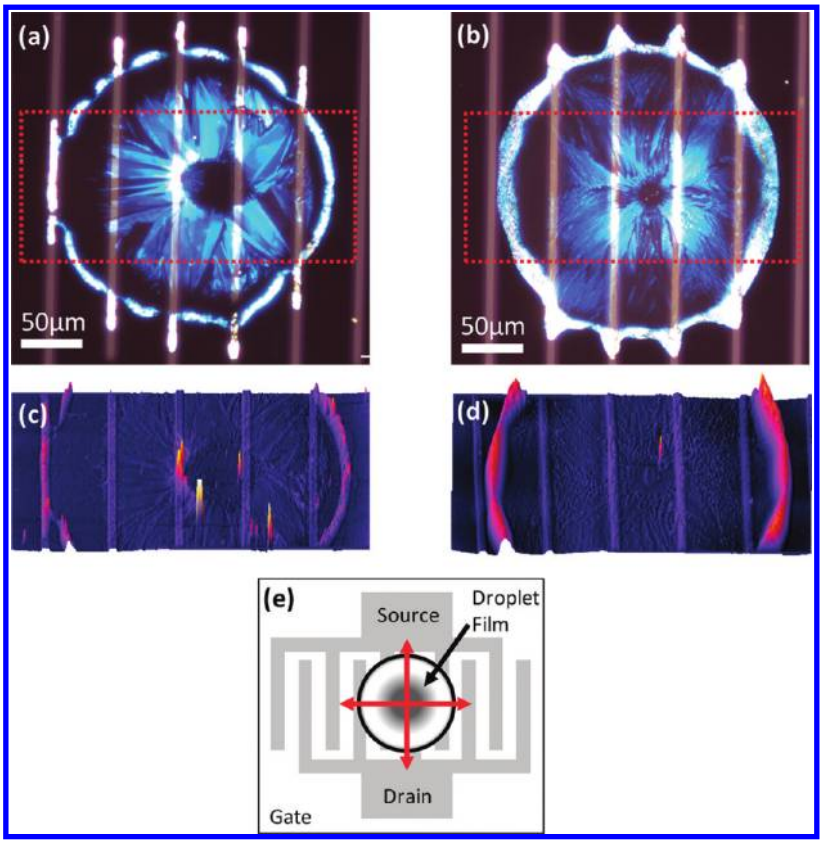

Figure 4. Cross-polarized optical images of (a) TIPS-Pentacene and (b) TIPS-Pentacene:PS OTFT with 40 μm channel length; (c,d) tapping mode AFM topography images of respective OTFTs taken from the areas highlighted in red; (e) schematic diagram showing the entire OTFT device structure (top view) with interdigitated source and drain contacts. Raman/AFM line scan directions indicated using red arrows.

increase in Raman scattering intensity. Between contacts 1 and 2, the topography is mostly flat and the Raman signal is close to zero. The Raman data indicate that there are small amounts of TIPS-Pentacene material in this region despite being barely visible in the topography. Between contacts 2 and 3, there is a uniform ~10 nm thick TIPS-Pentacene grain accompanied by a large increase in the Raman signal. Since the intensity of the short-axis mode (blue) is much higher than the long-axis mode (red), this suggests that the pentacene molecules in this grain are oriented predominantly parallel to the gold contacts. The mean molecular orientation determined by polarized Raman is shown on the figure. Between regions 3 and 4, the topography profile decreases and the Raman signal gradually decreases; however, it does not reach zero, suggesting the presence of a very thin layer of ordered TIPS-Pentacene. Between contacts 4 and 5, the topography profile is at its highest, which suggests a relatively thick TIPS-Pentacene region; however, note that the Raman signal is less than in region 2−3, indicating a less ordered TIPS-Pentacene region resulting from smaller grain sizes. It is important to emphasize that the Raman data do not correlate directly with the topography data; rather it provides information on the degree of order of the thin film down to the micrometer scale.

TIPS-Pentacene:PS. Equivalent measurements were performed on the TIPS-Pentacene:PS device as shown in Figure 5b. From the cross-polarized optical image (Figure 4b) and the AFM topography image (Figure 4d), it appears that the outermost PFBT-treated gold contacts act as a nucleation site for the crystalline grains, with the crystals growing radially inward toward the center. Once the initial nucleation has occurred, however, the crystals grow over the subsequent contacts without being disrupted. The thick edges of the droplet (from the topography profile) are correlated with strong integrated Raman intensity peaks at the edges and are caused by the accumulation of TIPS-Pentacene material in the coffee stain rim, due to the convective flow of solvent from the center to the edge.[32] Angle-dependent polarized Raman measurements of the coffee ring structure showed no anisotropy or preferential crystalline orientation, indicative of randomly oriented TIPS-Pentacene nanocrystals and supported by previous GIXRD studies.[33]

Along the channel width direction (vertical scan), the topography profile (Figure 5b (left)) is mostly homogeneous with an even coverage (~20 nm thick) across the device apart from the thick rim edges and a

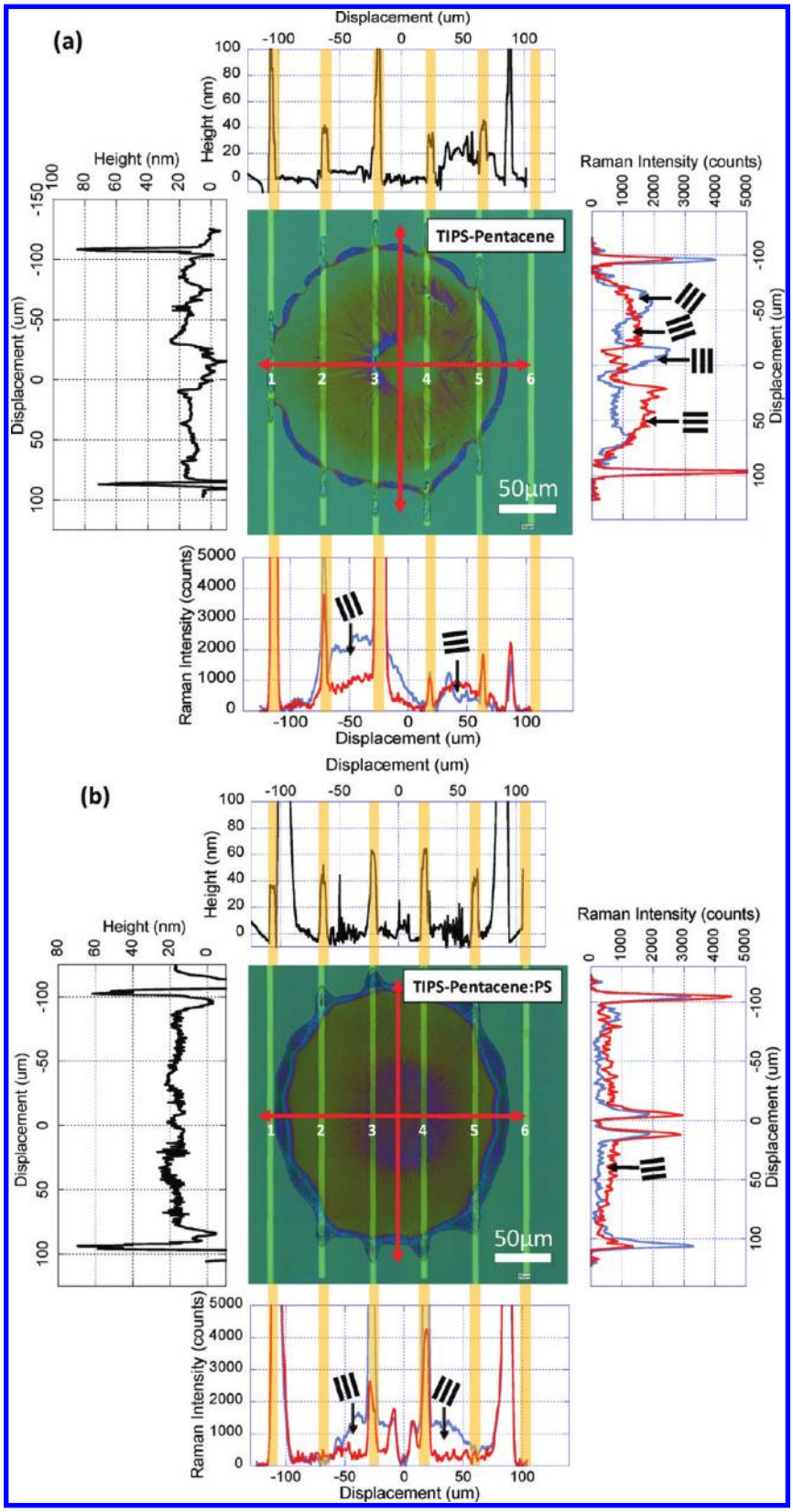

Figure 5. Raman/AFM characterization of (a) TIPS-Pentacene and (b) TIPS-Pentacene:PS OTFTs. Cross sections were first taken along the channel width direction (vertical arrows) showing topography (left) and Raman mode intensities (right). Both the C—C short-axis mode (blue) and C—C long-axis mode (red) are plotted in the Raman data. Subsequently, cross sections along the channel length direction (horizontal arrow) were taken showing topography (top) and Raman mode intensities (bottom). The locations of the interdigitated contacts are highlighted in gold. Mean pentacene backbone orientations measured from within selected domains (indicated by arrows) are shown on the Raman plots.

5−10 nm protrusion at the very center of the droplet encircled by an ~80 μm diameter ring of similar height. The Raman C−C long- and short-axis modes are almost uniform along the channel width (Figure 5b (right)). This indicates that, compared to the TIPS-Pentacene-only device, there is less pronounced variation in pentacene backbone orientation between grains. The topography scan along the channel length (Figure 5b (top) horizontal scan) again indicates that the film is, in general, flatter than that within the TIPS-Pentacene-only device (with the latter characterized by a more inhomogeneous coverage across the device).

In addition, another clear difference between the pure TIPS-Pentacene and the blend OTFTs is the Raman signal at the central point. For the blend sample, the Raman signal drops to zero in the very center (Figure 5b (right and bottom)), and the drop-off in signal is accompanied by a sharply defined region of high intensities for both the long and short pentacene backbone axes, immediately adjacent to the central point. The distinct absence of TIPS-Pentacene Raman signals from the central point tells us that no TIPS-Pentacene is present there (within the detection limits of the Raman system). However, there is not a void in the center; instead, we measure a slight protrusion which is seen from the AFM topography profile (Figure 5b (left and top)). From these two points, we infer the presence of a polystyrene-rich domain at the very center of the droplet film. We explain the accumulation of isotropic materials, in our case polystyrene, qualitatively by the three-stage drying dynamics of a polystyrene droplet.[31,34,35] First, the contact line of the deposited droplet is pinned to the surface during the initial stage of drying. The evaporation-rate profile, which is position-dependent over the droplet, gives rise to Marangoni forces which transport TIPS-Pentacene and polymer toward the contact line. At the contact line, the materials solidify and create the high coffee stain rims. During the second phase of drying, the contact line sweeps over the surface. In this phase, the long crystalline needles grow with the slipping contact line, from the perimeter radially inward toward the center. Close to the center, we measure an increase in Raman signals from an accumulation of TIPS-Pentacene molecules, oriented in all directions, with their pentacene backbone long axis parallel to the substrate plane. Recently, it was shown that the TIPS-Pentacene morphology depends on the speed at which the meniscus sweeps across the substrate, with thin, small-grained TIPS-Pentacene films observed for high meniscus speeds.[7] Similar effects are observed for other small-molecule/polymer blends with fast drying times yielding small grains.[12] We therefore conclude that the slipping speed of the contact line is highest during the second drying phase, just before it becomes pinned again. During the final stage of drying, the ink remains pinned until it totally solidifies and gives rise to the central protrusion. The presence of polystyrene at the center, for identical ink and processing conditions, has recently been reported elsewhere.[36]

Effect of Channel Length. In order to explore the effect of channel length on device morphology, TIPS-Pentacene and TIPS-Pentacene:PS devices with 5 μm channel length were probed using polarized Raman spectroscopy. Angle-dependent C−C (short-axis) mode plots were measured at regular intervals along the channel length (charge transport) direction, shown in Figure 6. All plots are to scale.

The first difference between the devices is the larger variation in intensity seen in the TIPS-Pentacene device relative to the blend device, indicating that the TIPS-Pentacene exhibits a larger variation in thickness across the film. Point 4 (at the center of the droplet) in both devices shows a very low C−C mode intensity due to the very low concentration of TIPS-Pentacene molecules in the center of both devices. The mean molecular orientation from the measured regions in both devices ranges from 60 to 110°, that is, predominantly perpendicular to the gold contacts. Again, the addition of polystyrene to the ink results in a more homogeneous film thickness for the 5 μm (as in the 40 μm) channel length devices. However, in the 5 μm channel length devices, blending does not significantly alter the variation in pentacene backbone orientation between grains because even in the TIPS-Pentacene-only device the orientation across the device is relatively uniform.

Morphology *versus* OTFT Performance. In order to compare the effect of blending TIPS-Pentacene with a polystyrene binder, charge transport properties from a large set of inkjet-printed OTFTs were analyzed, as described elsewhere,[36] using 63 pure TIPS-Pentacene and 73 TIPS-Pentacene:PS (2:1 by weight) transistors. The average saturation mobility calculated from the pure TIPS-Pentacene transistor data set is 0.22 $\pm$ 0.05 $cm^2/(V \cdot s)$, which is comparable to earlier reported values.[33,36,37] After blending, the average saturation mobility increases to 0.72 $\pm$ 0.17 $cm^2/(V \cdot s)$.

In addition to the increase in mobility, the presence of polystyrene strongly influences the threshold voltage (Figure 7), which decreases toward 0 V. In contrast, the pure TIPS-Pentacene transistors have higher threshold voltages (~2−7 V). This change in threshold voltage suggests an improvement in the semiconductor-dielectric interface, which is further supported by the smoother, more evenly distributed semiconductor films in the blend devices as observed from the AFM/Raman analysis.

Finally, the subthreshold slope is significantly steeper for the blend transistors (as steep as 67 mV/dec) than for the pure TIPS-Pentacene transistors. These characteristics again indicate that the interface between the semiconductor and dielectric is of excellent quality.[38,39] The Raman analysis shows that the blend

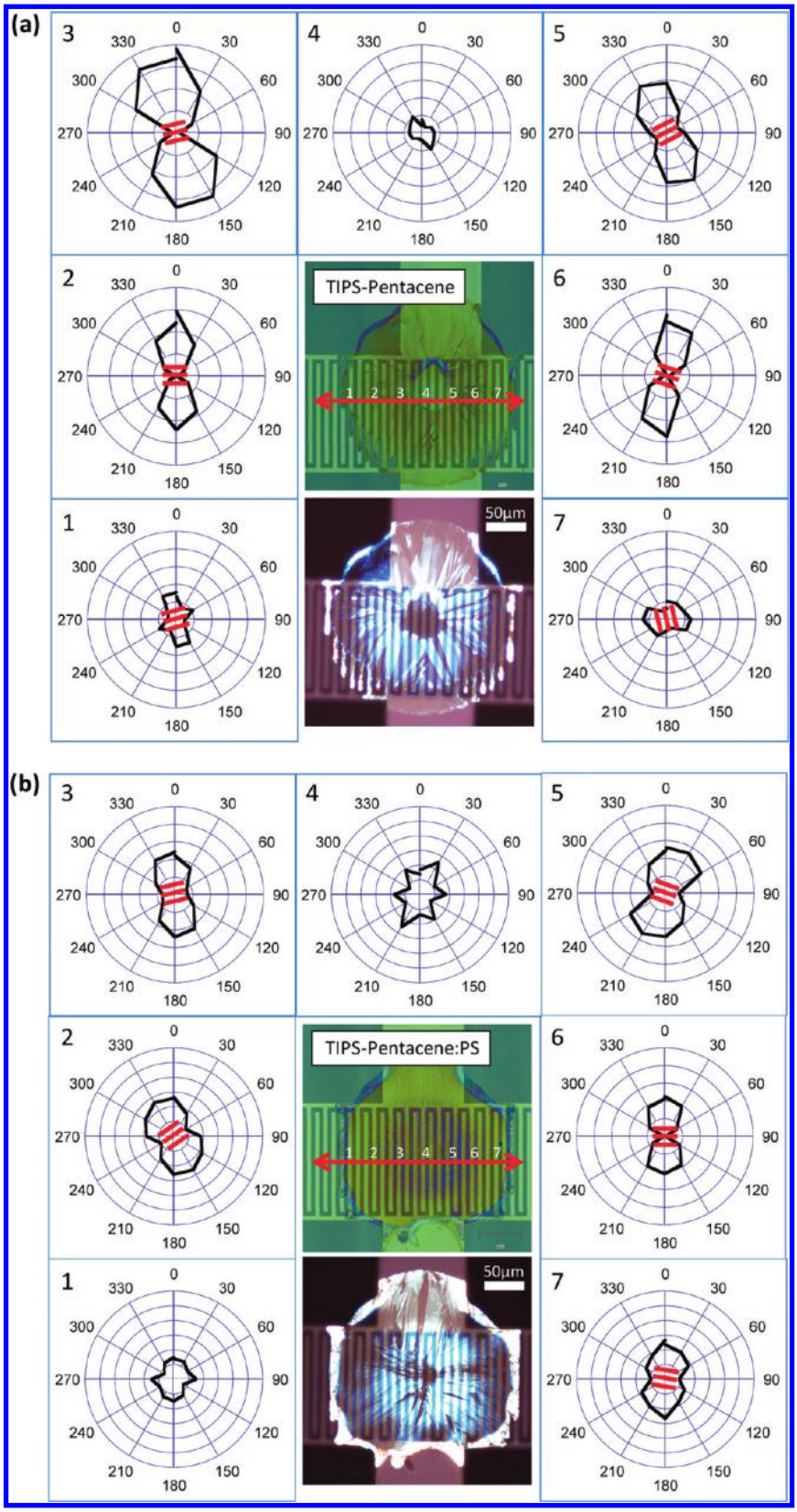

Figure 6. Polarized Raman plots for the C−C (short-axis) mode were taken at 7 points (indicated in the optical image) along the channel length direction from (a) TIPS-Pentacene and (b) TIPS-Pentacene:PS devices with 5 μm channel length. For this shorter channel length configuration, the TIPS-Pentacene domains showed a larger variation in intensity than in the TIPS-Pentacene:PS device, although both showed similar molecular orientation distributions.

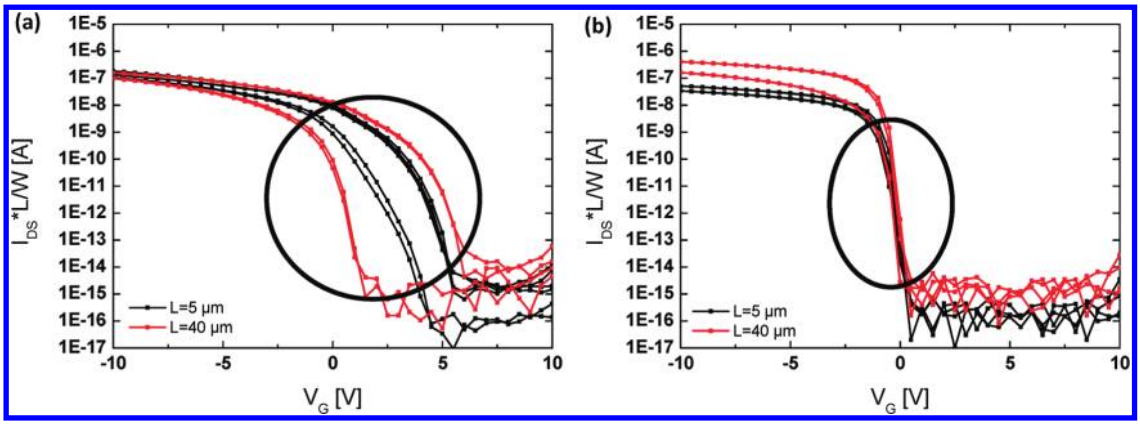

Figure 7. Transfer characteristics for (a) TIPS-Pentacene and (b) TIPS-Pentacene:PS devices with 5 μm (black) and 40 μm (red) channel lengths. Blending TIPS-Pentacene with polystyrene lowers the threshold voltage and increases the subthreshold slope of the devices (circled).

transistors have larger grains, with reduced variation in pentacene backbone orientation along both the channel width and channel length directions than the pure TIPS-Pentacene devices (Figure 5). The improved uniformity of the crystal orientation indicates that the crystallization process becomes less dependent on the different surfaces (*i.e.*, contacts and along the channel) with the addition of the polymer binder, resulting in a high-quality interface.

CONCLUSIONS

In this paper, we demonstrate angle-dependent polarized Raman spectroscopy as a noninvasive, nondestructive technique to determine the local degree of molecular order and orientation of the conjugated backbones in small-molecule thin films. The novelty of this technique lies in its ability to characterize the lateral morphology at a high spatial resolution (1 μm) as well as in completed device structures (*e.g.*, OTFTs). This technique was used to investigate the effect of polymer blending and surface treatments on the morphology of TIPS-Pentacene. Interestingly, the addition of an insulating polymer does not disrupt the $\pi-\pi$ stacking of the TIPS-Pentacene molecules; instead, the blending improves the TIPS-Pentacene morphology in terms of more uniform coverage across the device and less variation in pentacene backbone in-plane orientation. This is reflected in the OTFT performance as an improvement in saturation mobility (from 0.22 $cm^2/(V\cdot s)$ in pristine devices to 0.73 $cm^2/(V\cdot s)$ in blend devices) and a lower threshold voltage ($\sim$0 V) and steeper subthreshold slope (67 mV/dec), which both indicate an improved interface between the TIPS-Pentacene and channel dielectrics. In blend devices, the PFBT-treated gold contacts act as nucleating sites for the microcrystalline domains of TIPS-Pentacene that extend across the active channel region. The TIPS-Pentacene-only devices show highly ordered microcrystalline domains; however, there is evidence of larger domain-to-domain variation within the active channel of the device. For shorter channel lengths, the pentacene backbone orientations were similar for both TIPS-Pentacene and blend inks, however, as with longer channel lengths, blending stabilized the film thickness across the device. These results provide useful insights into the direct effects of ink composition and surface treatments on organic small-molecule morphology and its relation to device performance and can be readily applied to look at local changes in morphology in active devices or for mapping the molecular order and orientation at different regions of a device.

EXPERIMENTAL SECTION

Materials. TIPS-Pentacene was synthesized according to a previously reported procedure.[40] Amorphous polystyrene (PS), M_W = 9.58 kDa (M_n = 9.32 kDa, PDI = 1.03), was purchased from Fluka. 1,2,3,4-Tetrahydronaphthalene (tetralin, purchased from Merck) was used as the solvent. Inks were prepared with 20 mg of TIPS-Pentacene per milliliter tetralin or 20 mg of TIPS-Pentacene + 10 mg of PS per milliliter tetralin. The inks were inkjet-printed with microfab glass nozzles (type MJ-ATP-01-50-DLC, 50 μm orifice diameter). Droplets ($\sim$50 pL) were jetted on demand on the temperature-controlled substrate (70 °C).

Transistor Fabrication. Bottom-contact transistors were fabricated on silicon (n++) substrates with thermally grown silicon dioxide (200 nm). Gold source-drain electrodes (30 nm) with 2 nm Ti adhesion layer were patterned by photolithography. Pentafluorobenzenethiol (PFBT, 15 min immersion in 10 mM ethanol solution) was applied on source-drain electrodes. The oxide surface was treated with trichlorophenylsilane (TCPS, from gas phase, followed by short annealing at 100 °C).

Atomic Force Microscopy. Topographical information was obtained using an NT-MDT AFM system (Ntegra probe laboratory) in noncontact (tapping) mode.

Raman Measurements. Raman spectra were acquired using a Renishaw inVia Raman microscope and a 785 nm laser diode excitation source (50× objective, 30 s exposure time). For angle-dependent polarization measurements, a half-wave plate placed between the laser and the sample was used to rotate the orientation of the plane-polarized laser light. Raman spectra

were taken at 10° rotation intervals using an automated rotating optical mount, which allowed for accurate control of the polarization angle of the incident laser light. For the Raman line scans, the polarization angle was fixed at an angle perpendicular to the gold contacts. Collected spectra were then analyzed for peak intensities. All samples were measured in air and required no special preparation for the measurement.

Raman Simulation. In order to interpret the Raman spectrum of TIPS-Pentacene, vibrational frequencies were calculated using the Gaussian 09 quantum chemical calculation package.[41] A TIPS-Pentacene molecule was first geometrically optimized in the virtual gas phase followed by a vibrational frequency calculation using density functional theory (DFT) at the B3LYP level of theory[42] and using the 6-31G* basis set.

Electrical Characterization. Device characteristics were measured at room temperature in inert atmosphere using an Agilent 4155C semiconductor parameter analyzer. The field-effect mobilities (μ_{sat}) of our transistors in the saturation regime were calculated from eq 1 as follows, with $V_{SD} = -1$ and -10 V, respectively:

$$\mu_{sat}(V_g) = \frac{2L}{WC}\left(\frac{\partial\sqrt{I_d(V_g)}}{\partial V_g}\right)^2 \quad (1)$$

where C_i is the capacitance per unit area of the gate dielectric layer, and L and W are channel length and width, respectively.

Acknowledgment. This work was supported by the Val O'Donoghue Scholarship in Natural Sciences, CDT CASE studentship, the World Class University (WCU) Project (Grant No. R32-10051), the European Community's Seventh Framework Programme (FP7/2007-2013) under Grant Agreement No. 212311 of the ONE-P project and Grant Agreement No. 216546 of the FLAME project.

Supporting Information Available: TIPS-Pentacene Raman mode assignments using quantum chemical calculations. This material is available free of charge *via* the Internet at http://pubs.acs.org.

REFERENCES AND NOTES

1. Hamilton, R.; Smith, J.; Ogier, S.; Heeney, M.; Anthony, J. E.; McCulloch, I.; Veres, J.; Bradley, D. D. C.; Anthopoulos, T. D. High-Performance Polymer-Small Molecule Blend Organic Transistors. *Adv. Mater.* **2009**, *21*, 1166–1171.
2. Madec, M.-B.; Crouch, D.; Llorente, G. R.; Whittle, T. J.; Geoghegan, M.; Yeates, S. G. Organic Field Effect Transistors from Ambient Solution Processed Low Molar Mass Semiconductor-Insulator Blends. *J. Mater. Chem.* **2008**, *18*, 3230–3236.
3. Ohe, T.; Kuribayashi, M.; Yasuda, R.; Tsuboi, A.; Nomoto, K.; Satori, K.; Itabashi, M.; Kasahara, J. Solution-Processed Organic Thin-Film Transistors with Vertical Nanophase Separation. *Appl. Phys. Lett.* **2008**, *93*, 053303.
4. Park, S. K.; Jackson, T. N.; Anthony, J. E.; Mourey, D. A. High Mobility Solution Processed 6,13-Bis(triisopropyl-silylethynyl) Pentacene Organic Thin Film Transistors. *Appl. Phys. Lett.* **2007**, *91*, 063514.
5. Hamadani, B. H.; Gundlach, D. J.; McCulloch, I.; Heeney, M. Undoped Polythiophene Field-Effect Transistors with Mobility of 1 $cm^2V^{-1}s^{-1}$. *Appl. Phys. Lett.* **2007**, *91*, 243512.
6. Kim, C. S.; Lee, S.; Gomez, E. D.; Anthony, J. E.; Loo, Y.-L. Solvent-Dependent Electrical Characteristics and Stability of Organic Thin-Film Transistors with Drop Cast Bis-(triisopropylsilylethynyl) pentacene. *Appl. Phys. Lett.* **2008**, *93*, 103302.
7. Sele, C. W.; Kjellander, B. K. C.; Niesen, B.; Thornton, M. J.; van der Putten, J. B. P. H; Myny, K.; Wondergem, H. J.; Moser, A.; Resel, R.; van Breemen, A. J. J. M.; *et al.* Controlled Deposition of Highly Ordered Soluble Acene Thin Films: Effect of Morphology and Crystal Orientation on Transistor Performance. *Adv. Mater.* **2009**, *21*, 4926–4931.
8. Kjellander, B. K. C.; Smaal, W. T. T.; Anthony, J. E.; Gelinck, G. H. Inkjet Printing of TIPS-PEN on Soluble Polymer Insulating Films: A Route to High-Performance Thin-Film Transistors. *Adv. Mater.* **2010**, *22*, 4612–4616.
9. deGans, B. J.; Duineveld, P. C.; Schubert, U. S. Inkjet Printing of Polymers: State of the Art and Future Developments. *Adv. Mater.* **2004**, *16*, 203–213.
10. Madec, M.-B.; Smith, P. J.; Malandraki, A.; Wang, N.; Korvink, J. G.; Yeates, S. G. Enhanced Reproducibility of Inkjet Printed Organic Thin Film Transistors Based on Solution Processable Polymer-Small Molecule Blends. *J. Mater. Chem.* **2010**, *20*, 9155–9160.
11. Smith, J.; Hamilton, R.; Heeney, M.; de Leeuw, D. M.; Cantatore, E.; Anthony, J. E.; McCulloch, I.; Bradley, D. D. C.; Anthopoulos, T. D. High-Performance Organic Integrated Circuits Based on Solution Processable Polymer-Small Molecule Blends. *Appl. Phys. Lett.* **2008**, *93*, 253301.
12. Smith, J.; Hamilton, R.; Qi, Y.; Kahn, A.; Bradley, D. D. C.; Heeney, M.; McCulloch, I.; Anthopoulos, T. D. The Influence of Film Morphology in High-Mobility Small-Molecule:Polymer Blend Organic Transistors. *Adv. Funct. Mater.* **2010**, *20*, 2330–2337.
13. Smith, J.; Hamilton, R.; McCulloch, I.; Stingelin-Stutzmann, N.; Heeney, M.; Bradley, D. D. C.; Anthopoulos, T. D. Solution-Processed Organic Transistors Based on Semiconducting Blends. *J. Mater. Chem.* **2010**, *20*, 2562–2574.
14. Kang, J.; Shin, N.; Jang, D. Y.; Prabhu, V. M.; Yoon, D. Y. Structure and Properties of Small Molecule-Polymer Blend Semiconductors for Organic Thin Film Transistors. *J. Am. Chem. Soc.* **2008**, *130*, 12273–12275.
15. Smith, J.; Heeney, M.; McCulloch, I.; Malik, J. N.; Stingelin, N.; Bradley, D. D. C.; Anthopoulos, T. D. Percolation Behaviour in High Mobility P-Channel Polymer/Small-Molecule Blend Organic Field-Effect Transistors. *Org. Electron.* **2011**, *12*, 143–147.
16. Kim, J.-S.; Ho, P. K. H.; Murphy, C. E.; Friend, R. H. Phase Separation in Polyfluorene-Based Conjugated Polymer Blends: Lateral and Vertical Analysis of Blend Spin-Cast Thin Films. *Macromolecules* **2004**, *37*, 2861–2871.
17. Kim, J. S.; Ho, P. K. H.; Murphy, C. E.; Baynes, N.; Friend, R. H. Nature of Non-emissive Black Spots in Polymer Light-Emitting Diodes by *In-Situ* Micro-Raman Spectroscopy. *Adv. Mater.* **2002**, *14*, 206–209.
18. Donley, C. L.; Zaumseil, J.; Andreasen, J. W.; Nielsen, M. M.; Sirringhaus, H.; Friend, R. H.; Kim, J. S. Effects of Packing Structure on the Optoelectronic and Charge Transport Properties in Poly(9,9-di-*n*-octylfluorene-*alt*-benzothiadiazole). *J. Am. Chem. Soc.* **2005**, *127*, 12890–12899.
19. Schmidtke, J. P.; Kim, J.-S.; Gierschner, J.; Silva, C.; Friend, R. H. Optical Spectroscopy of a Polyfluorene Copolymer at High Pressure: Intra- and Intermolecular Interactions. *Phys. Rev. Lett.* **2007**, *99*, 167401.
20. Winfield, J. M.; Donley, C. L.; Friend, R. H.; Kim, J.-S. Probing Thin-Film Morphology of Conjugated Polymers by Raman Spectroscopy. *J. Appl. Phys.* **2010**, *107*, 024902.
21. Kim, J.-S.; Ho, P. K. H.; Murphy, C. E.; Seeley, A. J. A. B.; Grizzi, I.; Burroughes, J. H.; Friend, R. H. Electrical Degradation of Triarylamine-Based Light-Emitting Polymer Diodes Monitored by Micro-Raman Spectroscopy. *Chem. Phys. Lett.* **2004**, *386*, 2–7.
22. Soltzberg, L. J.; Slinker, J. D.; Flores-Torres, S.; Bernards, D. A.; Malliaras, G. G.; Abruña, H. D.; Kim, J.-S.; Friend, R. H.; Kaplan, M. D.; Goldberg, V. Identification of a Quenching Species in Ruthenium Tris-bipyridine Electroluminescent Devices. *J. Am. Chem. Soc.* **2006**, *128*, 7761–7764.
23. Kotarba, S.; Jung, J.; Kowalska, A.; Marszalek, T.; Kozanecki, M.; Miskiewicz, P.; Mas-Torrent, M.; Rovira, C.; Veciana, J.; Puigmarti-Luis, J.; *et al.* Anisotropy in Structural and Physical Properties in Tetrathiafulvalene Derivatives-Based Zone-Cast Layers As Seen by Raman Spectroscopy, UV-Visible Spectroscopy, and Field Effect Measurements. *J. Appl. Phys.* **2010**, *108*, 014504.
24. Cheng, H. L.; Chou, W. Y.; Kuo, C. W.; Wang, Y. W.; Mai, Y. S.; Tang, F. C.; Chu, S. W. Influence of Electric Field on Microstructures of Pentacene Thin-Films in Field-Effect Transistors. *Adv. Funct. Mater.* **2008**, *18*, 285–293.
25. Jentzsch, T.; Juepner, H. J.; Brzezinka, K. W.; Lau, A. Efficiency of Optical Second Harmonic Generation from

Pentacene Films of Different Morphology and Structure. *Thin Solid Films* **1998**, *315*, 273–280.
26. Brillante, A.; Della Valle, R. G.; Farina, L.; Girlando, A.; Masino, M.; Venuti, E. Raman Phonon Spectra of Pentacene Polymorphs. *Chem. Phys. Lett.* **2002**, *357*, 32–36.
27. Chen, J. H.; Martin, D. C.; Anthony, J. E. Morphology and Molecular Orientation of Thin-Film Bis(triisopropylsilylethynyl) Pentacene. *J. Mater. Res.* **2007**, *22*, 1701–1709.
28. Li, X.; Kjellander, B. K. C.; Anthony, J. E.; Bastiaansen, C. W. M.; Broer, D. J.; Gelinck, G. H. Azeotropic Binary Solvent Mixtures for Preparation of Organic Single Crystals. *Adv. Funct. Mater.* **2009**, *19*, 3610–3617.
29. Kim, S.-o.; An, T. K.; Chen, J.; Kang, I.; Kang, S. H.; Chung, D. S.; Park, C. E.; Kim, Y.-H.; Kwon, S.-K. H-Aggregation Strategy in the Design of Molecular Semiconductors for Highly Reliable Organic Thin Film Transistors. *Adv. Funct. Mater.* **2011**, *21*, 1616–1623.
30. Lim, J. A.; Lee, H. S.; Lee, W. H.; Cho, K. Control of the Morphology and Structural Development of Solution-Processed Functionalized Acenes for High-Performance Organic Transistors. *Adv. Funct. Mater.* **2009**, *19*, 1515–1525.
31. Lim, J.; Lee, W.; Kwak, D.; Cho, K. Evaporation-Induced Self-Organization of Inkjet-Printed Organic Semiconductors on Surface-Modified Dielectrics for High-Performance Organic Transistors. *Langmuir* **2009**, *25*, 5404–5410.
32. Deegan, R. D.; Bakajin, O.; Dupont, T. F.; Huber, G.; Nagel, S. R.; Witten, T. A. Capillary Flow as the Cause of Ring Stains from Dried Liquid Drops. *Nature* **1997**, *389*, 827–829.
33. Lim, J. A.; Lee, W. H.; Lee, H. S.; Lee, J. H.; Park, Y. D.; Cho, K. Self-Organization of Ink-Jet-Printed Triisopropylsilylethynyl Pentacene *via* Evaporation-Induced Flows in a Drying Droplet. *Adv. Funct. Mater.* **2008**, *18*, 229–234.
34. Fukai, J.; Ishizuka, H.; Sakai, Y.; Kaneda, M.; Morita, M.; Takahara, A. Effects of Droplet Size and Solute Concentration on Drying Process of Polymer Solution Droplets Deposited on Homogeneous Surfaces. *Int. J. Heat Mass Transfer* **2006**, *49*, 3561–3567.
35. Deegan, R. D.; Bakajin, O.; Dupont, T. F.; Huber, G.; Nagel, S. R.; Witten, T. A. Contact Line Deposits in an Evaporating Drop. *Phys. Rev. E* **2000**, *62*, 756–765.
36. Li, X.; Smaal, W. T. T.; Kjellander, C.; van der Putten, B.; Gualandris, K.; Smits, E. C. P.; Anthony, J.; Broer, D. J.; Blom, P. W. M.; Genoe, J.; *et al.* Charge Transport in High-Performance Ink-Jet Printed Single-Droplet Organic Transistors Based on a Silylethynyl Substituted Pentacene/Insulating Polymer Blend. *Org. Electron.* **2011**, *12*, 1319–1327.
37. Lee, S. H.; Choi, M. H.; Han, S. H.; Choo, D. J.; Jang, J.; Kwon, S. K. High-Performance Thin-Film Transistor with 6,13-Bis(triisopropylsilylethynyl) Pentacene by Inkjet Printing. *Org. Electron.* **2008**, *9*, 721–726.
38. Myny, K.; De Vusser, S.; Steudel, S.; Janssen, D.; Muller, R.; De Jonge, S.; Verlaak, S.; Genoe, J.; Heremans, P. Self-Aligned Surface Treatment for Thin-Film Organic Transistors. *Appl. Phys. Lett.* **2006**, *88*, 222103.
39. Jin, Y.; Rang, Z.; Nathan, M. I.; Ruden, P. P.; Newman, C. R.; Frisbie, C. D. Pentacene Organic Field-Effect Transistor on Metal Substrate with Spin-Coated Smoothing Layer. *Appl. Phys. Lett.* **2004**, *85*, 4406–4408.
40. Anthony, J. E.; Brooks, J. S.; Eaton, D. L.; Parkin, S. R. Functionalized Pentacene: Improved Electronic Properties from Control of Solid-State Order. *J. Am. Chem. Soc.* **2001**, *123*, 9482–9483.
41. Frisch, M. J.; Trucks, G. W.; Schlegel, H. B.; Scuseria, G. E.; Robb, M. A.; Cheeseman, J. R.; Scalmani, G.; Barone, V.; Mennucci, B.; Petersson, G. A., *et al. Gaussian 09*, revision A.02; Gaussian, Inc.: Wallingford, CT, 2009.
42. Becke, A. D. Density-Functional Thermochemistry. III. The Role of the Exact Exchange. *J. Chem. Phys.* **1993**, *98*, 5648–5652.